Supporting Information: The relativistic hydrogen-like atom in a finite magnetic field

Benedikt Menges,[†] Bang C. Huynh,[‡] Lucas Visscher,[†] and Ansgar Pausch[*,†]

†*Department of Chemistry and Pharmaceutical Sciences, Vrije Universiteit Amsterdam, De Boelelaan 1108, 1081 HZ Amsterdam, The Netherlands*

‡*Physical and Theoretical Chemistry Laboratory, Department of Chemistry, University of Oxford, Oxford OX1 3QZ, United Kingdom*

E-mail: a.i.pausch@vu.nl

1 Overview

In this Supporting Information (SI), we present additional details and results concerning our investigation on the relativistic hydrogen-like atom in a finite magnetic field. We have performed calculations on the following systems: H, Li^{2+}, Na^{10+}, K^{18+}, Cu^{28+}, Ag^{46+}, Au^{78+}, and Rn^{85+}. Only selected results were presented in the main document, but in this SI we will present all results. It is thus structured as follows: In sec. 2, we show a detailed derivation the characters of spinors in the double group $\mathscr{C}_{\infty h}$. In sec. 3, we present the computational details for the calculations shown in this SI. Sec. 4 compares analytical results in the field-free case to our results. This was shown for some systems in the main document, but is shown for all systems here. In sec. 5, the comparison between non-relativistic calculations and the results of Rösner et al.[1] is shown for two states not discussed in the main document. Sec. 6 then shows the transition from anomalous Zeeman effect to the Paschen–Back limit for the second and third shell of all hydrogen-like atoms investigated here. Finally, sec. 7 demonstrates the basis set convergences of the systems discussed

here, particularly with respect to how many angular momentum functions ($l_{\max}$) are needed for quantitative predictions in dependence of the magnetic fields strength.

2 Characters of spinors in $\mathscr{C}_{\infty h}$

Consider spinors of half-integer angular momentum j arising from the coupling of a spatial part of integer angular momentum l and a spin part of angular momentum $1/2$. The Clebsch–Gordon coupling rule tells us that, given j, there are only two possible values for l: $l = j + 1/2$ and $l = j - 1/2$, which correspond to two kinds of spinors of angular momentum j:

$$|j,m_j\rangle^+ = \sum_{m_l,m_s} |j+1/2,m_l\rangle\,|1/2,m_s\rangle\,\langle j+1/2,1/2,m_l,m_s|j,m_j\rangle\,, \tag{1a}$$

$$|j,m_j\rangle^- = \sum_{m_l,m_s} |j-1/2,m_l\rangle\,|1/2,m_s\rangle\,\langle j-1/2,1/2,m_l,m_s|j,m_j\rangle\,, \tag{1b}$$

where $\langle j \pm 1/2, 1/2, m_l, m_s | j, m_j \rangle$ are the Clebsch–Gordon coefficients. Noting that the Clebsch–Gordon coefficients are only non-zero for $m_l + m_s = m_j$, we can simplify the above summations as

$$|j,m_j\rangle^+ = \sum_{m_s} |j+1/2,m_j-m_s\rangle\,|1/2,m_s\rangle\,\langle j+1/2,1/2,m_j-m_s,m_s|j,m_j\rangle\,, \tag{2a}$$

$$|j,m_j\rangle^- = \sum_{m_s} |j-1/2,m_j-m_s\rangle\,|1/2,m_s\rangle\,\langle j-1/2,1/2,m_j-m_s,m_s|j,m_j\rangle\,. \tag{2b}$$

We write these succinctly as

$$|j,m_j\rangle^a = \begin{cases} |j,m_j\rangle^+ \equiv |l = j+1/2, j, m_j\rangle\,, \\ |j,m_j\rangle^- \equiv |l = j-1/2, j, m_j\rangle\,, \end{cases} \tag{3}$$

as also shown in the main text. We seek to determine the transformations of these spinors under the actions of the symmetry operations in the group $\mathscr{C}_{\infty h}$. These are the proper rotations through an

angle ϕ about the z-axis $\hat{C}_z(\phi)$, the spatial inversion $\hat{i}$, the reflection in the horizontal mirror plane $\hat{\sigma}_h$, and the improper rotations about the z-axis $\hat{S}_z(\phi)$.

2.1 Proper rotations

First, let us consider the action of a general rotation about an axis $\hat{\mathbf{n}}$ through an angle φ, which we shall denote $\hat{R}(\varphi\hat{\mathbf{n}})$, on a general function $|j,m_j\rangle$:

$$\hat{R}(\varphi\hat{\mathbf{n}})\,|j,m_j\rangle = \sum_{m'_j} |j,m'_j\rangle\, D^{(j)}_{m'_j m_j}[\hat{R}(\varphi\hat{\mathbf{n}})], \tag{4}$$

where $\mathbf{D}^{(j)}[\hat{R}(\varphi\hat{\mathbf{n}})]$ is the representation matrix of $\hat{R}(\varphi\hat{\mathbf{n}})$ in the basis $\{|j,m_j\rangle, m_j = -j,\ldots,j\}$. It turns out that for a rotation about the z-axis $\hat{C}_z(\phi)$, $\mathbf{D}^{(j)}$ is always diagonal:

$$D^{(j)}_{m'_j m_j}[\hat{C}_z(\phi)] = D^{(j)}_{m'_j m_j}[\hat{R}(\phi\hat{\mathbf{z}})] = \exp\left(-\mathrm{i}\phi m_j\right)\delta_{m'_j m_j}. \tag{5}$$

Thus,

$$\hat{C}_z(\phi)\,|j,m_j\rangle^{+} = \exp\left(-\mathrm{i}\phi m_j\right)|j,m_j\rangle^{+}, \tag{6a}$$

$$\hat{C}_z(\phi)\,|j,m_j\rangle^{-} = \exp\left(-\mathrm{i}\phi m_j\right)|j,m_j\rangle^{-}, \tag{6b}$$

which implies that the way the spinors $|j,m_j\rangle^{\pm}$ transform under $\hat{C}_z(\phi)$ is determined by their m_j values. The characters of $\hat{C}_z(\phi)$ for the spinors are highlighted in magenta.

2.2 Spatial inversion

The transformation of the spatial functions $|l,m_l\rangle$ under inversion is straightforward:

$$\hat{i}\,|l,m_l\rangle = (-1)^l\,|l,m_l\rangle\,. \tag{7}$$

However, the transformation of $|1/2, m_s\rangle$ under inversion is gauge-dependent. In what follows, we shall choose the *Pauli gauge*[2] such that

$$\hat{i}|1/2, m_s\rangle = |1/2, m_s\rangle\,. \tag{8}$$

Hence, from eq. (2), we obtain

$$\hat{i}|j, m_j\rangle^+ = (-1)^{j+1/2}\,|j, m_j\rangle^+\,, \tag{9a}$$

$$\hat{i}|j, m_j\rangle^- = (-1)^{j-1/2}\,|j, m_j\rangle^-\,, \tag{9b}$$

which implies that the way the spinors $|j, m_j\rangle^\pm$ transform under $\hat{i}$ is determined by their spatial angular momentum quantum numbers $l = j \pm 1/2$. The characters of $\hat{i}$ for the spinors are highlighted in magenta.

2.3 Reflection in the horizontal mirror plane

Noting that $\hat{\sigma}_h = \hat{C}_z(\pi)\hat{i}$, we can combine the results from eqs. (6) and (9) to obtain

$$\hat{C}_z(\pi)\hat{i}\,|j, m_j\rangle^+ = \exp\!\big(-\mathrm{i}\pi m_j\big)(-1)^{j+1/2}\,|j, m_j\rangle^+ = (-1)^{j+1/2-m_j}\,|j, m_j\rangle^+\,, \tag{10a}$$

$$\hat{C}_z(\pi)\hat{i}\,|j, m_j\rangle^- = \exp\!\big(-\mathrm{i}\pi m_j\big)(-1)^{j-1/2}\,|j, m_j\rangle^- = (-1)^{j-1/2-m_j}\,|j, m_j\rangle^-\,, \tag{10b}$$

which implies that the way the spinors $|j, m_j\rangle^\pm$ transform under $\hat{\sigma}_h$ is determined by both their spatial angular momentum quantum numbers $l = j \pm 1/2$ and their m_j values. Since $l = j \pm 1/2$ is an integer but m_j is a half-integer, the factors $(-1)^{j\pm1/2-m_j} = (-1)^{l-m_j}$ must therefore be imaginary. The characters of $\hat{\sigma}_h$ for the spinors are highlighted in magenta.

2.4 Improper rotations

Finally, noting that $\hat{S}_z(\phi) = \hat{C}_z(\phi)\hat{\sigma}_h$ and the projective factor[2] $[\hat{C}_z(\phi), \hat{\sigma}_h] = -1$, we can combine the results from eqs. (6) and (10) to obtain

$$\hat{S}_z(\phi)\,|j,m_j\rangle^+ = -\exp\left(-\mathrm{i}\phi m_j\right)(-1)^{j+1/2-m_j}\,|j,m_j\rangle^+\,, \tag{11a}$$

$$\hat{S}_z(\phi)\,|j,m_j\rangle^- = -\exp\left(-\mathrm{i}\phi m_j\right)(-1)^{j-1/2-m_j}\,|j,m_j\rangle^-\,. \tag{11b}$$

The characters of $\hat{S}_z(\phi)$ for the spinors are highlighted in magenta.

3 Computational Details

We reiterate the computational details discussed in the main document here. Large even-tempered basis sets were chosen such that chemical accuracy (errors of less than 1 kcal/mol $\approx 1.6 \cdot 10^{-3} E_\mathrm{h}$) can be obtained over a large window of magnetic field strengths, usually up to $1\,B_0$ for all investigated states. For the data presented in this work, we have chosen the basis sets detailed in table 1. Furthermore, we assessed the basis set convergence with respect to the highest required angular momentum function l_max. The results are presented in sec. 7.

Table 1: Information about the even-tempered basis sets used in this work. The limit l_max indicates the largest spherical harmonic used, with s-type functions being $l = 0$ and so forth. For all spherical harmonics, the same smallest exponent ζ_min and largest exponent ζ_max were used. Finally, Δ signifies the spacing between exponents

Element	l_max	ζ_min	ζ_max	Δ
H	18	10^{-6}	10^{7}	2.0
Li^{2+}	11	10^{-6}	10^{8}	1.7
Na^{10+}	11	10^{-5}	10^{9}	1.7
K^{18+}	11	10^{-6}	10^{9}	2.0
Cu^{28+}	11	10^{-6}	10^{9}	2.0
Ag^{46+}	11	10^{-5}	10^{10}	2.0
Au^{78+}	10	10^{-5}	10^{10}	2.0
Rn^{85+}	6	10^{-5}	10^{10}	1.7

4 Comparison with analytical results in the field-free case

4.1 The hydrogen atom

Table 2: Electronic solutions for the relativistic hydrogen atom in the absence of an external magnetic field. Here, our results for the lowest three shells are compared to the analytic values, alongside the difference ΔE.

Level	This work in $[E_\mathrm{h}]$	Analytic value in $[E_\mathrm{h}]$	ΔE in $[E_\mathrm{h}]$
$1s_{1/2}$	-0.5000066841	-0.5000066566	$-2.75 \cdot 10^{-8}$
$2s_{1/2}$	-0.1250020773	-0.1250020802	$+2.91 \cdot 10^{-9}$
$2p_{1/2}$	-0.1250020564	-0.1250020802	$+2.38 \cdot 10^{-8}$
$2p_{3/2}$	-0.1250004004	-0.1250004160	$+1.56 \cdot 10^{-8}$
$3s_{1/2}$	-0.0555561630	-0.0555562952	$+1.32 \cdot 10^{-7}$
$3p_{1/2}$	-0.0555562217	-0.0555562952	$+7.35 \cdot 10^{-8}$
$3p_{3/2}$	-0.0555557324	-0.0555558021	$+6.96 \cdot 10^{-8}$
$3d_{3/2}$	-0.0555557752	-0.0555558021	$+2.68 \cdot 10^{-8}$
$3d_{5/2}$	-0.0555556123	-0.0555556377	$+2.54 \cdot 10^{-8}$

4.2 The Li^{2+} ion

Table 3: Electronic solutions for the relativistic Li^{2+} ion in the absence of an external magnetic field. Here, our results for the lowest three shells are compared to the analytic values, alongside the difference ΔE.

Level	This work in $[E_\mathrm{h}]$	Analytic value in $[E_\mathrm{h}]$	ΔE in $[E_\mathrm{h}]$
$1s_{1/2}$	-4.5005392014	-4.5005392992	$+9.78 \cdot 10^{-8}$
$2s_{1/2}$	-1.1251684215	-1.1251685330	$+1.12 \cdot 10^{-7}$
$2p_{1/2}$	-1.1251684885	-1.1251685330	$+4.45 \cdot 10^{-8}$
$2p_{3/2}$	-1.1250336377	-1.1250337001	$+6.25 \cdot 10^{-8}$
$3s_{1/2}$	-0.5000598881	-0.5000599214	$+3.33 \cdot 10^{-8}$
$3p_{1/2}$	-0.5000599087	-0.5000599214	$+1.27 \cdot 10^{-8}$
$3p_{3/2}$	-0.5000199320	-0.5000199705	$+3.86 \cdot 10^{-8}$
$3d_{3/2}$	-0.5000199847	-0.5000199705	$-1.42 \cdot 10^{-8}$
$3d_{5/2}$	-0.5000066635	-0.5000066566	$-6.89 \cdot 10^{-9}$

4.3 The Na^{10+} ion

Table 4: Electronic solutions for the relativistic Na^{10+} ion in the absence of an external magnetic field. Here, our results for the lowest three shells are compared to the analytic values, alongside the difference ΔE.

Level	This work in $[E_h]$	Analytic value in $[E_h]$	ΔE in $[E_h]$
$1s_{1/2}$	-60.597772081	-60.597771882	$-1.99 \cdot 10^{-7}$
$2s_{1/2}$	-15.155558755	-15.155558648	$-1.07 \cdot 10^{-7}$
$2p_{1/2}$	-15.155558734	-15.155558648	$-8.62 \cdot 10^{-8}$
$2p_{3/2}$	-15.131095854	-15.131095951	$+9.65 \cdot 10^{-8}$
$3s_{1/2}$	-6.7330840249	-6.7330840304	$+5.51 \cdot 10^{-9}$
$3p_{1/2}$	-6.7330844560	-6.7330840304	$-4.26 \cdot 10^{-7}$
$3p_{3/2}$	-6.7258351376	-6.7258348530	$-2.85 \cdot 10^{-7}$
$3d_{3/2}$	-6.7258352217	-6.7258348530	$-3.69 \cdot 10^{-7}$
$3d_{5/2}$	-6.7234261149	-6.7234258214	$-2.93 \cdot 10^{-7}$

4.4 The K^{18+} ion

Table 5: Electronic solutions for the relativistic K^{18+} ion in the absence of an external magnetic field. Here, our results for the lowest three shells are compared to the analytic values, alongside the difference ΔE.

Level	This work in $[E_h]$	Analytic value in $[E_h]$	ΔE in $[E_h]$
$1s_{1/2}$	-181.37591080	-181.37591079	$-1.27 \cdot 10^{-8}$
$2s_{1/2}$	-45.398851050	-45.398854709	$+3.66 \cdot 10^{-6}$
$2p_{1/2}$	-45.398851112	-45.398854709	$+3.60 \cdot 10^{-6}$
$2p_{3/2}$	-45.179343759	-45.179347625	$+3.87 \cdot 10^{-6}$
$3s_{1/2}$	-20.152775057	-20.152832307	$+5.72 \cdot 10^{-5}$
$3p_{1/2}$	-20.152781526	-20.152832307	$+5.08 \cdot 10^{-5}$
$3p_{3/2}$	-20.087715668	-20.087767300	$+5.16 \cdot 10^{-5}$
$3d_{3/2}$	-20.087754779	-20.087767300	$+1.25 \cdot 10^{-5}$
$3d_{5/2}$	-20.066264176	-20.066276530	$+1.24 \cdot 10^{-5}$

4.5 The Cu^{28+} ion

Table 6: Electronic solutions for the relativistic Cu^{28+} ion in the absence of an external magnetic field. Here, our results for the lowest three shells are compared to the analytic values, alongside the difference ΔE.

Level	This work in $[E_\mathrm{h}]$	Analytic value in $[E_\mathrm{h}]$	ΔE in $[E_\mathrm{h}]$
$1s_{1/2}$	-425.31641989	-425.31642693	$+7.04 \cdot 10^{-6}$
$2s_{1/2}$	-106.63183856	-106.63185004	$+1.15 \cdot 10^{-5}$
$2p_{1/2}$	-106.63184036	-106.63185004	$+9.68 \cdot 10^{-6}$
$2p_{3/2}$	-105.42089639	-105.42090626	$+9.87 \cdot 10^{-6}$
$3s_{1/2}$	-47.256595711	-47.256774609	$+1.79 \cdot 10^{-4}$
$3p_{1/2}$	-47.256697003	-47.256774609	$+7.76 \cdot 10^{-5}$
$3p_{3/2}$	-46.897564093	-46.897647141	$+8.30 \cdot 10^{-5}$
$3d_{3/2}$	-46.897620406	-46.897647141	$+2.67 \cdot 10^{-5}$
$3d_{5/2}$	-46.780463446	-46.780490234	$+2.68 \cdot 10^{-5}$

4.6 The Ag^{46+} ion

Table 7: Electronic solutions for the relativistic Ag^{46+} ion in the absence of an external magnetic field. Here, our results for the lowest three shells are compared to the analytic values, alongside the difference ΔE.

Level	This work in $[E_\mathrm{h}]$	Analytic value in $[E_\mathrm{h}]$	ΔE in $[E_\mathrm{h}]$
$1s_{1/2}$	-1139.0447346	-1139.0447654	$+3.08 \cdot 10^{-5}$
$2s_{1/2}$	-286.95357302	-286.95361288	$+3.99 \cdot 10^{-5}$
$2p_{1/2}$	-286.95358728	-286.95361288	$+2.56 \cdot 10^{-5}$
$2p_{3/2}$	-278.18545784	-278.18548566	$+2.78 \cdot 10^{-5}$
$3s_{1/2}$	-126.54824534	-126.54863376	$+3.88 \cdot 10^{-4}$
$3p_{1/2}$	-126.54848860	-126.54863376	$+1.45 \cdot 10^{-4}$
$3p_{3/2}$	-123.94442650	-123.94459755	$+1.71 \cdot 10^{-4}$
$3d_{3/2}$	-123.94453077	-123.94459755	$+6.68 \cdot 10^{-5}$
$3d_{5/2}$	-123.12580035	-123.12586693	$+6.66 \cdot 10^{-5}$

4.7 The Au^{78+} ion

Table 8: Electronic solutions for the relativistic Au^{78+} ion in the absence of an external magnetic field. Here, our results for the lowest three shells are compared to the analytic values, alongside the difference ΔE.

Level	This work in $[E_h]$	Analytic value in $[E_h]$	ΔE in $[E_h]$
$1s_{1/2}$	-3434.5834071	-3434.5867743	$+3.37 \cdot 10^{-3}$
$2s_{1/2}$	-879.22890910	-879.22952862	$+6.20 \cdot 10^{-4}$
$2p_{1/2}$	-879.22944126	-879.22952862	$+8.74 \cdot 10^{-5}$
$2p_{3/2}$	-797.03949549	-797.03954833	$+5.28 \cdot 10^{-5}$
$3s_{1/2}$	-381.26969513	-381.27054961	$+8.54 \cdot 10^{-4}$
$3p_{1/2}$	-381.26991625	-381.27054961	$+6.33 \cdot 10^{-4}$
$3p_{3/2}$	-356.77688929	-356.77764344	$+7.54 \cdot 10^{-4}$
$3d_{3/2}$	-356.77740484	-356.77764344	$+2.39 \cdot 10^{-4}$
$3d_{5/2}$	-349.98329784	-349.98356131	$+2.63 \cdot 10^{-4}$

4.8 The Rn^{85+} ion

Table 9: Electronic solutions for the relativistic Rn^{85+} ion in the absence of an external magnetic field. Here, our results for the lowest three shells are compared to the analytic values, alongside the difference ΔE.

Level	This work in $[E_h]$	Analytic value in $[E_h]$	ΔE in $[E_h]$
$1s_{1/2}$	-4158.4183046	-4158.4243359	$+6.03 \cdot 10^{-3}$
$2s_{1/2}$	-1070.0941611	-1070.0952493	$+1.09 \cdot 10^{-3}$
$2p_{1/2}$	-1070.0951564	-1070.0952493	$+9.28 \cdot 10^{-5}$
$2p_{3/2}$	-948.45139903	-948.45139553	$-3.51 \cdot 10^{-6}$
$3s_{1/2}$	-461.41067503	-461.41100214	$+3.27 \cdot 10^{-4}$
$3p_{1/2}$	-461.41096418	-461.41100214	$+3.80 \cdot 10^{-5}$
$3p_{3/2}$	-425.13635279	-425.13635814	$+5.35 \cdot 10^{-6}$
$3d_{3/2}$	-425.13636326	-425.13635814	$-5.12 \cdot 10^{-6}$
$3d_{5/2}$	-415.48523001	-415.48522557	$-4.44 \cdot 10^{-6}$

5 Non-relativistic hydrogen in a magnetic field

In this section, we compare the non-relativistic results obtained with our code against the results obtained by Rösner et al.[1] We have shown these for most states we investigated in the main document and do not wish to reiterate the results here. Two more states were investigated, though: $2\Sigma_u$ and $2\Pi_u^+$. The respective comparison is shown in figure 1. The trend is similar to what we noticed in the main document. These are highly excited states, and we observe good agreement up to field strengths of approximately $1\,B_0$. At this point, we diverge from the results of Rösner et al. At this point, their group uses a Landau basis (indicated in green hollow points in the figure), which is very accurate for highly excited states in very strong magnetic fields. For a more detailed discussion, please see the main document.

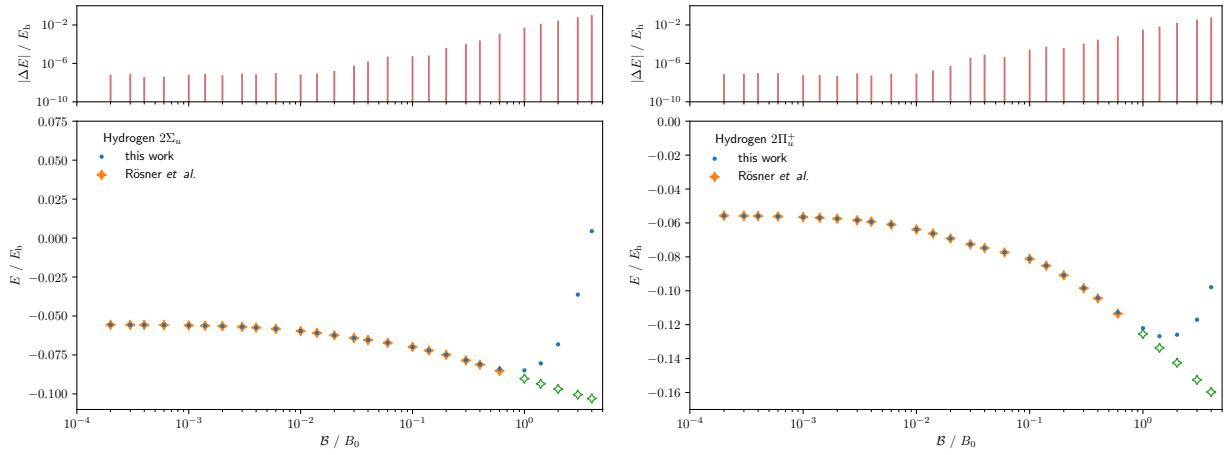

Figure 1: Comparison between non-relativistic calculations performed in the context of this work and those performed by Rösner et al. in Ref. 1. Shown here are deviations for the following states: (a) $2\Sigma_u$, (b) $2\Pi_u^+$. Reference values are accurate up to at most $10^{-6}\,E_\mathrm{h}$, which is indicated in gray above the graphs.

6 Relativistic hydrogen-like atoms in finite magnetic fields

In this section, we present the transition from anomalous Zeeman effect to Paschen–Back and finally Landau limit. We show results for all systems. In figures 2 and 3, we show the results of the *ungerade* states in the second shell ($2p$ orbitals), many of which have already been shown in the main document. In figures 4 and 5, we show the results of the *gerade* states in the third shell ($3d$ orbitals). The spin-orbit coupling strength is smaller for $3d$ orbitals, and thus they are only well-separated for very heavy elements. We can clearly see from figures 5c and 5d for Au^{78+} and Rn^{85+} in particular that we are still well within the anomalous Zeeman limit and thus relativistic effective core potentials (RECPs) would likely still be useful for a description of such states in strong magnetic fields. For elements up to Ag^{46+}, the $3d$ shell should not be considered to be part of the core region in terms of magnetic perturbation. Further studies on RECPs for heavy elements (not their hydrogen-like counterparts) will be the subject of future work.

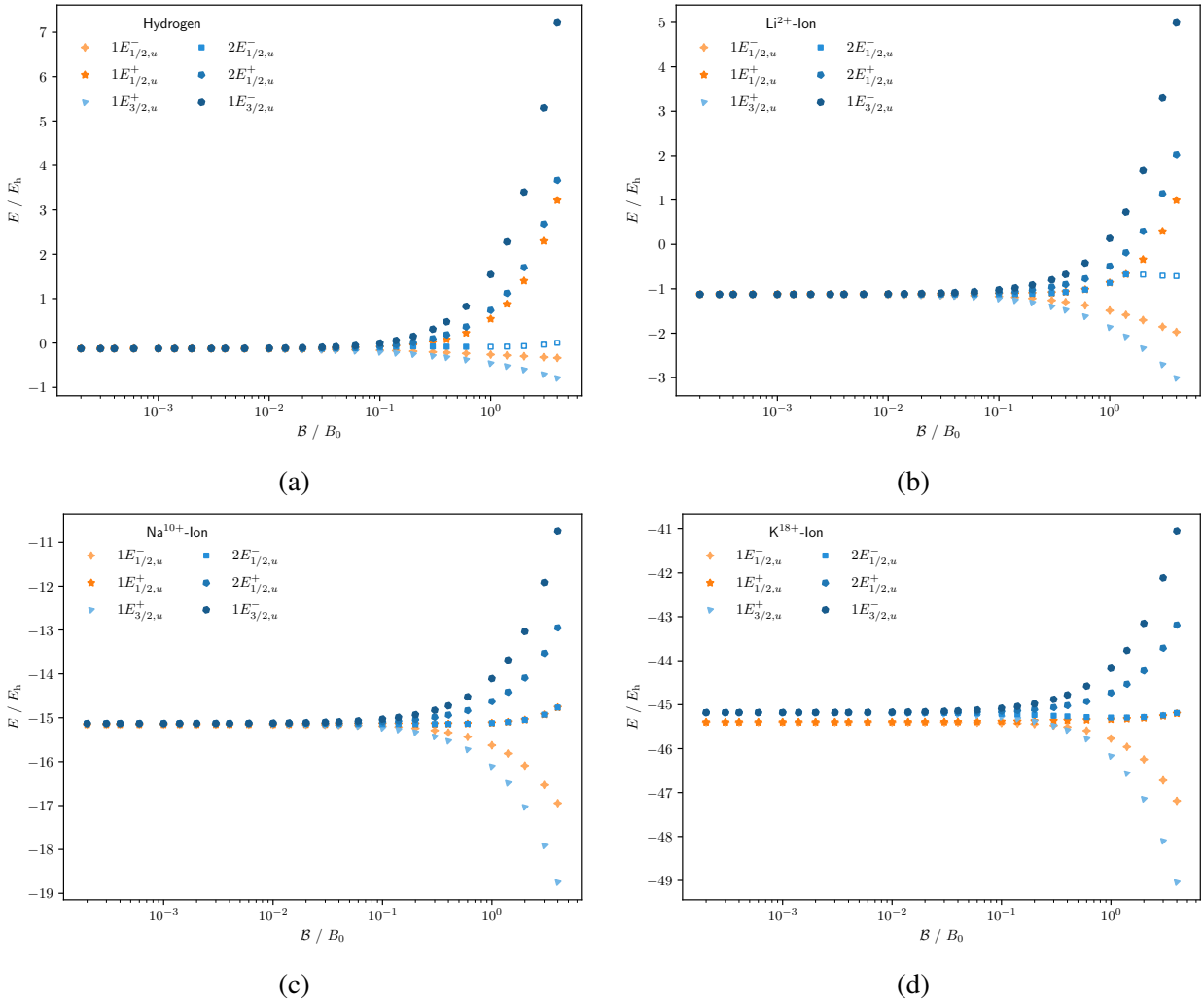

Figure 2: Transition from the anomalous Zeeman limit to the Paschen–Back and Landau limits for (a) hydrogen, (b) Li^{2+}, (c) Na^{10+}, and (d) K^{18+}. We show the $2p$ orbitals here.

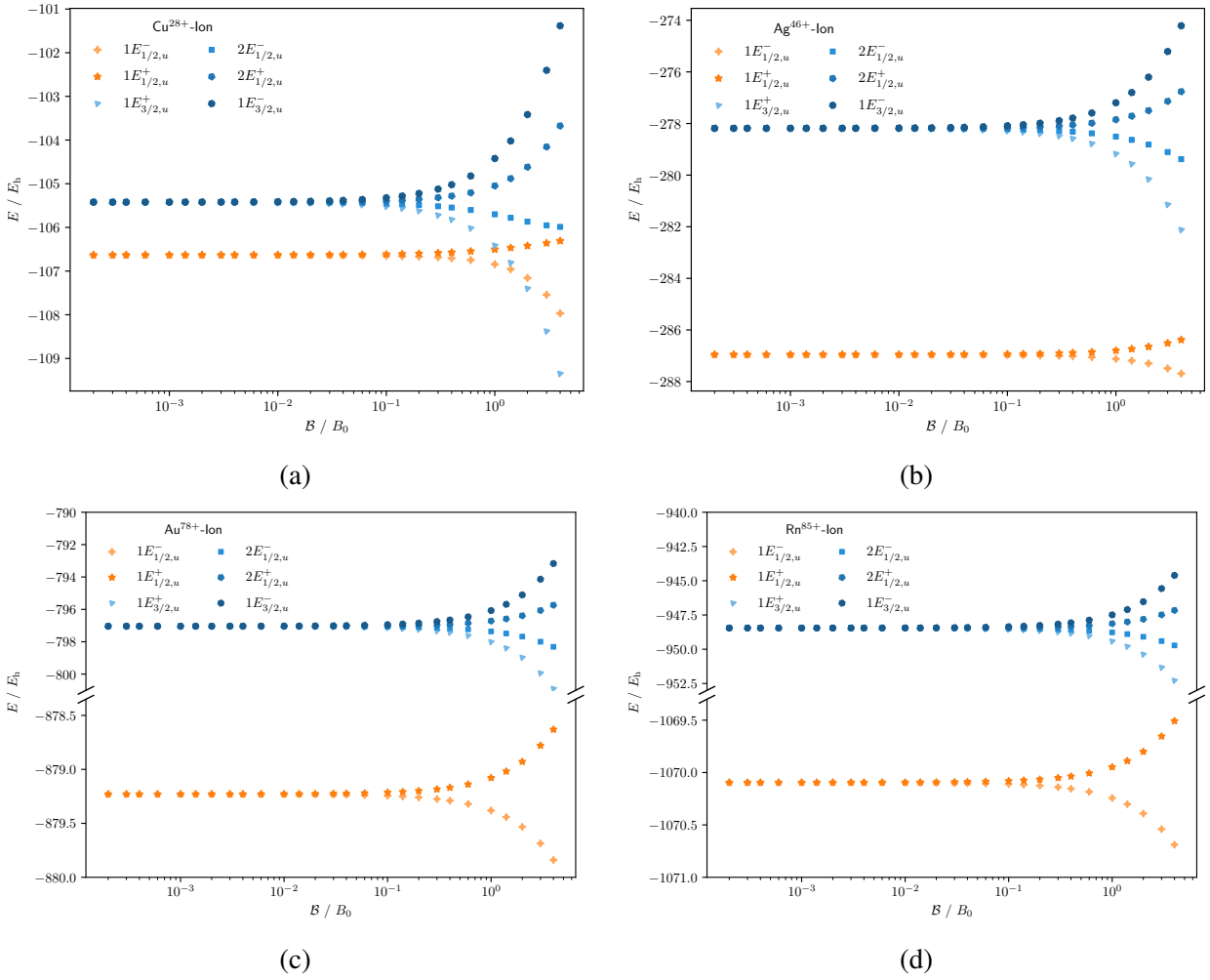

Figure 3: Transition from the anomalous Zeeman limit to the Paschen–Back and Landau limits for (a) Cu^{28+}, (b) Ag^{46+}, (c) Au^{78+}, and (d) Rn^{85+}. We show the $2p$ orbitals here.

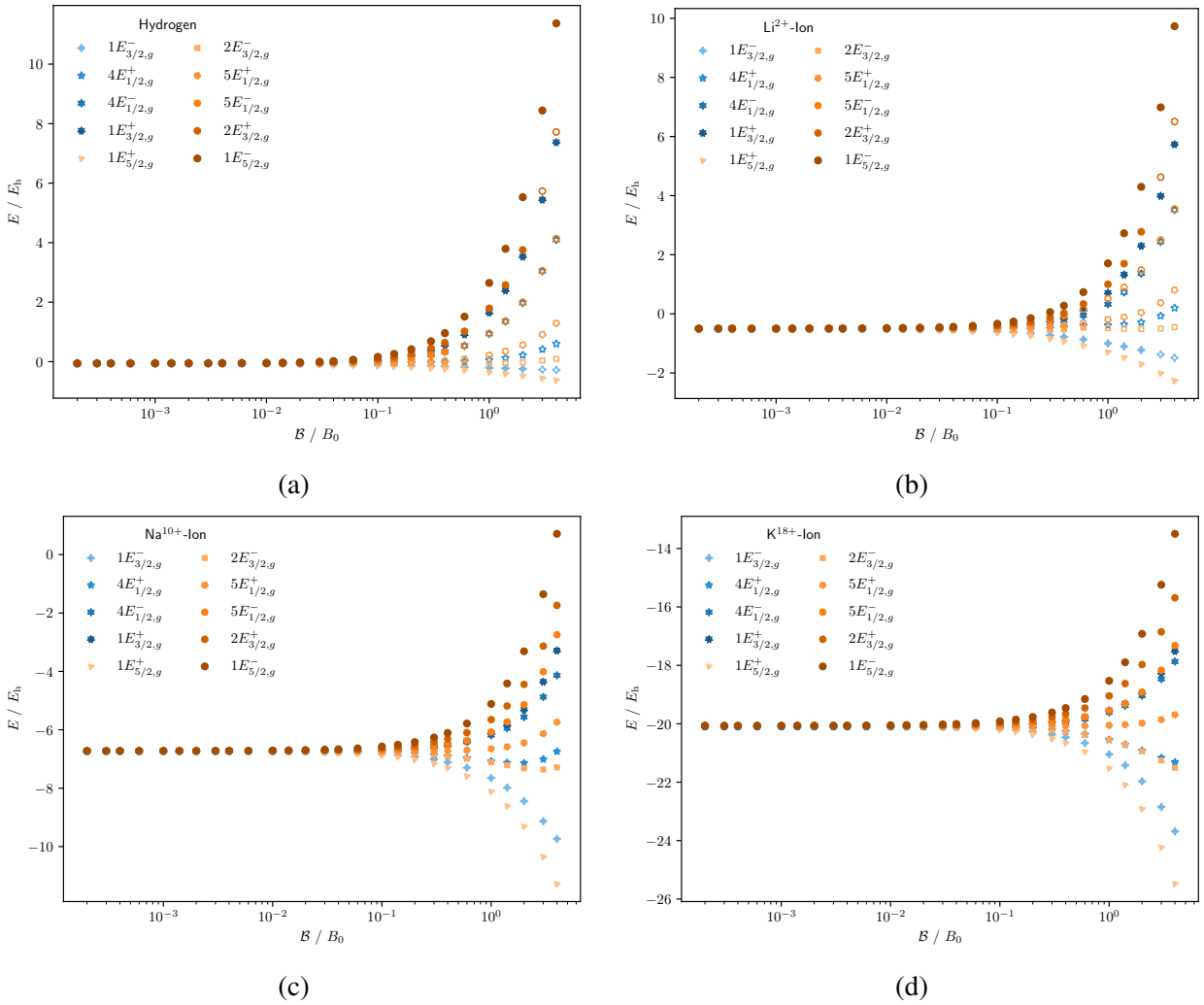

Figure 4: Transition from the anomalous Zeeman limit to the Paschen–Back and Landau limits for (a) hydrogen, (b) Li^{2+}, (c) Na^{10+}, and (d) K^{18+}. We show the $3d$ orbitals here.

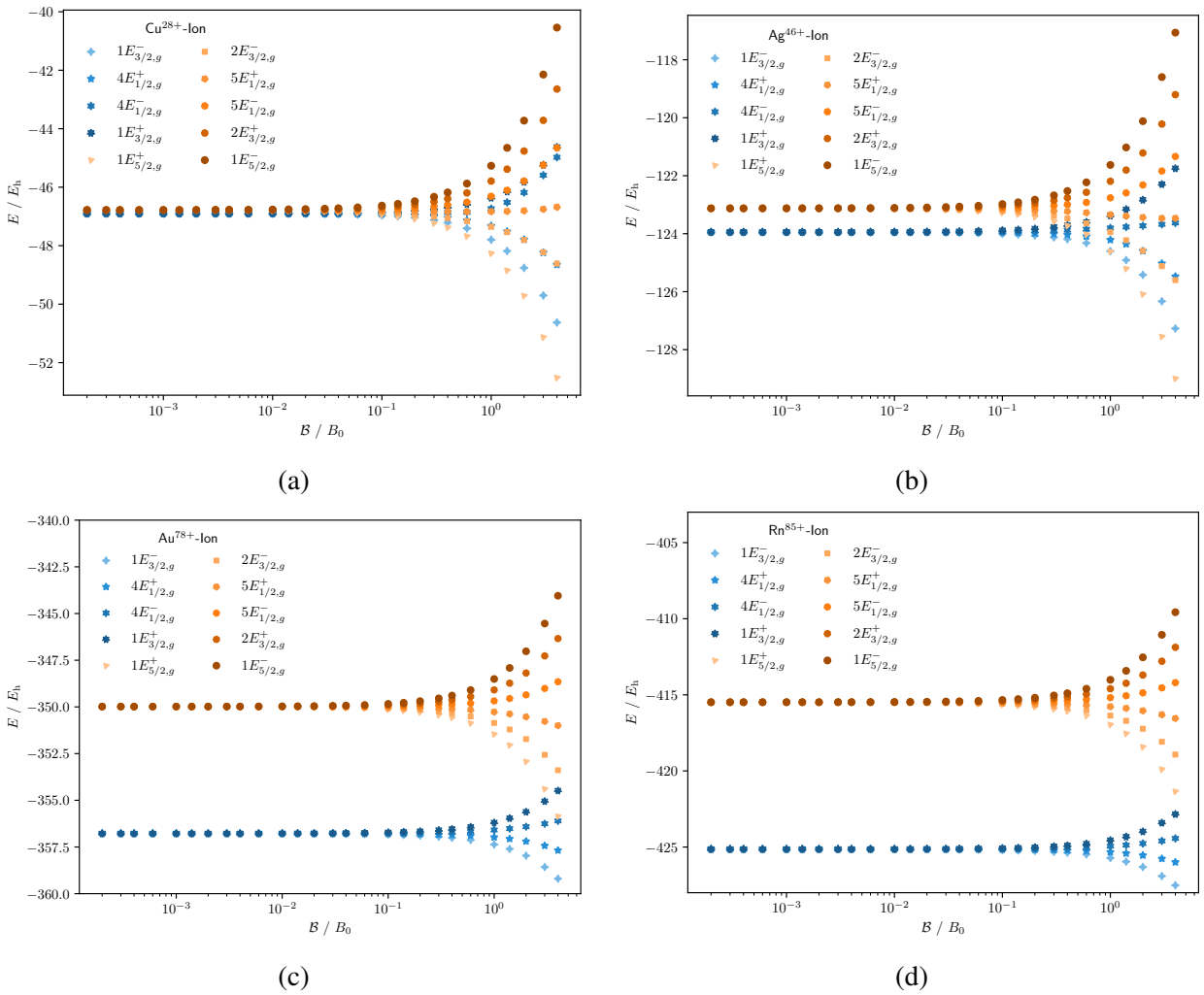

Figure 5: Transition from the anomalous Zeeman limit to the Paschen–Back and Landau limits for (a) Cu^{28+}, (b) Ag^{46+}, (c) Au^{78+}, and (d) Rn^{85+}. We show the 3*d* orbitals here.

7 Basis set convergence

In this last section of the Supporting Information, we will show the basis set convergence of all states investigated in this context of this work. We only calculate the convergence with respect to the required maximum angular momentum function $l_{\max}$. We only consider angular momentum functions up to the limit shown in table 1. The general trend we observe here is clear: heavier elements need less angular momentum functions. Coulomb forces and spin-orbit coupling are much stronger for heavier elements, and thus much higher magnetic field strengths are required for the more cylindrical shape observed in the Landau limit.

It should be noted that problems with basis set convergence are essentially only observed for hydrogen and Li^{2+}, particularly for highly excited states. For all heavier elements, we could confirm that all states investigated in this work are converged with respect to $l_{\max}$. For heavier elements, we often do not need any higher angular momentum functions. This underlines again that the core region is only slightly perturbed by the presence of a strong external magnetic field, while the valence region is heavily affected. It is therefore a reasonable assumption that RECPs will likely work out of the box for heavy elements if implemented with LAOs.

It should be noted that for very heavy elements and large basis sets, we could sometimes observe that our kinetic energy matrix $\mathbf{\Pi}$ is not always positive-definite, even though we used the canonical orthogonalization scheme described for the overlap matrix $\mathbf{S}$ in the main document. This only occurred for Au^{78+} for $l_{\max} > 10$ and for Rn^{85+} for $l_{\max} > 6$, which is why we restricted our results for Au^{78+} and Rn^{85+} such that we are not affected here. While this issue could in principle be solved, this lies beyond the scope of this work.

7.1 The hydrogen atom

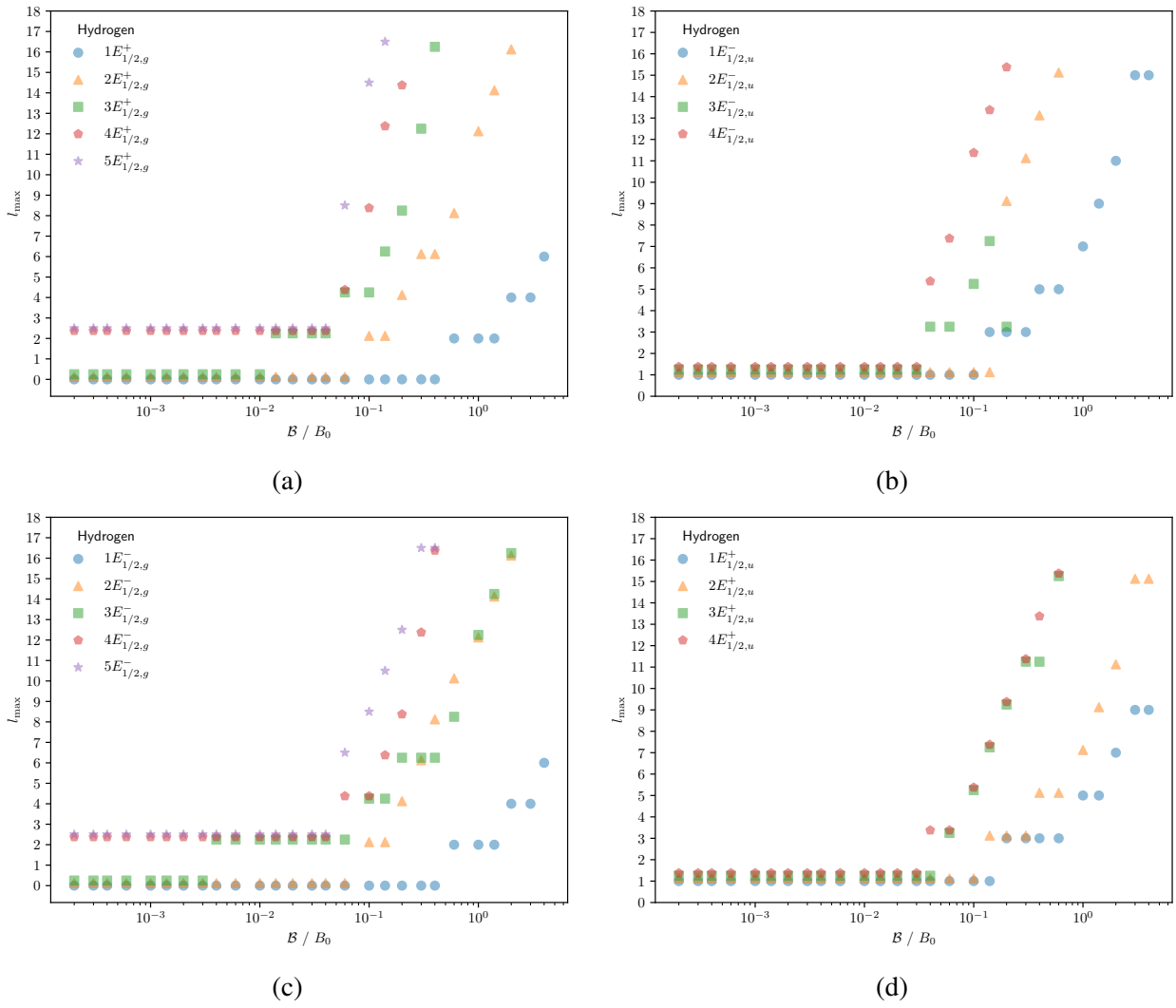

Figure 6: Basis set convergence for the $E_{1/2}$ states of hydrogen.

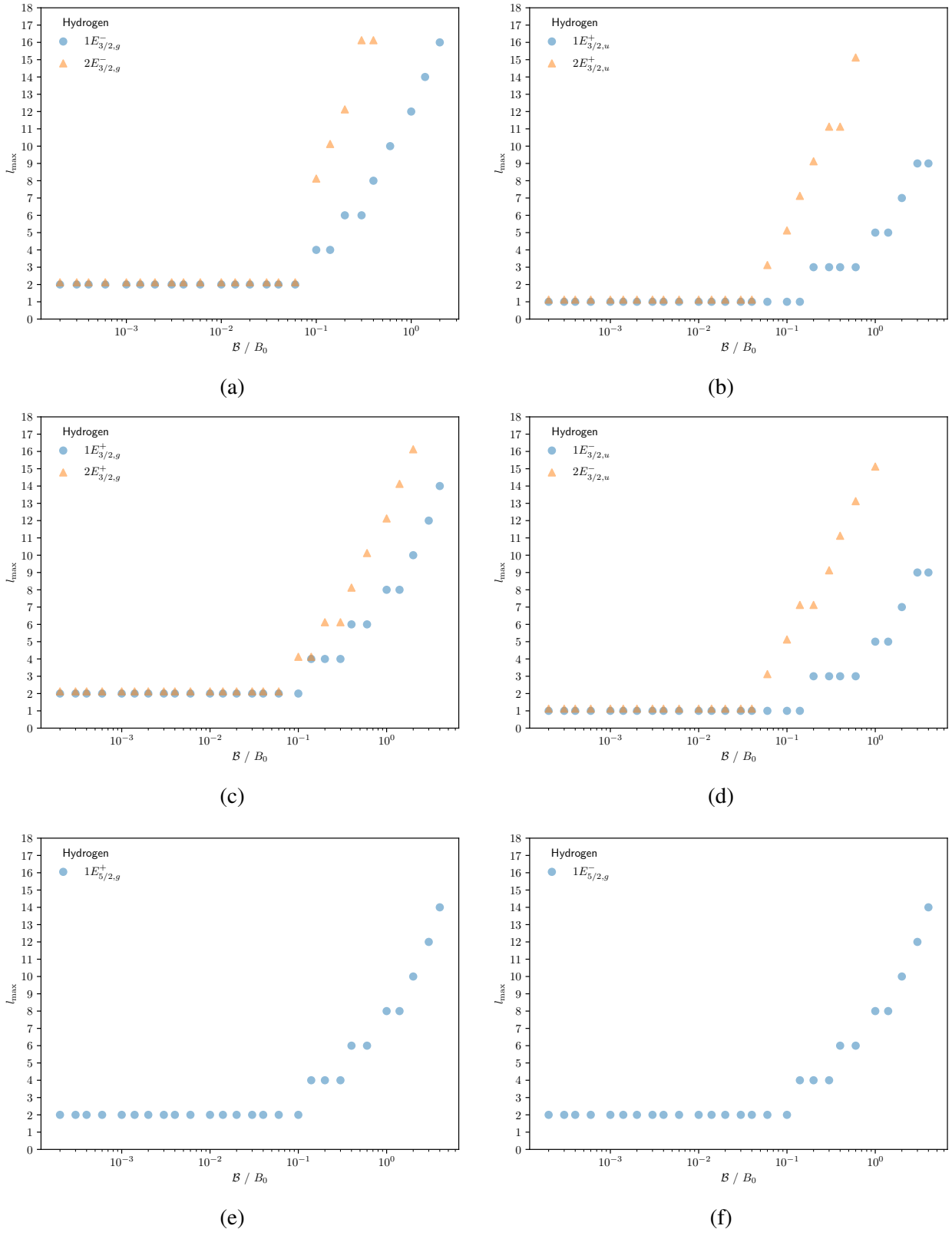

Figure 7: Basis set convergence for the $E_{3/2}$ and $E_{5/2}$ states of hydrogen.

7.2 The Li^{2+} ion

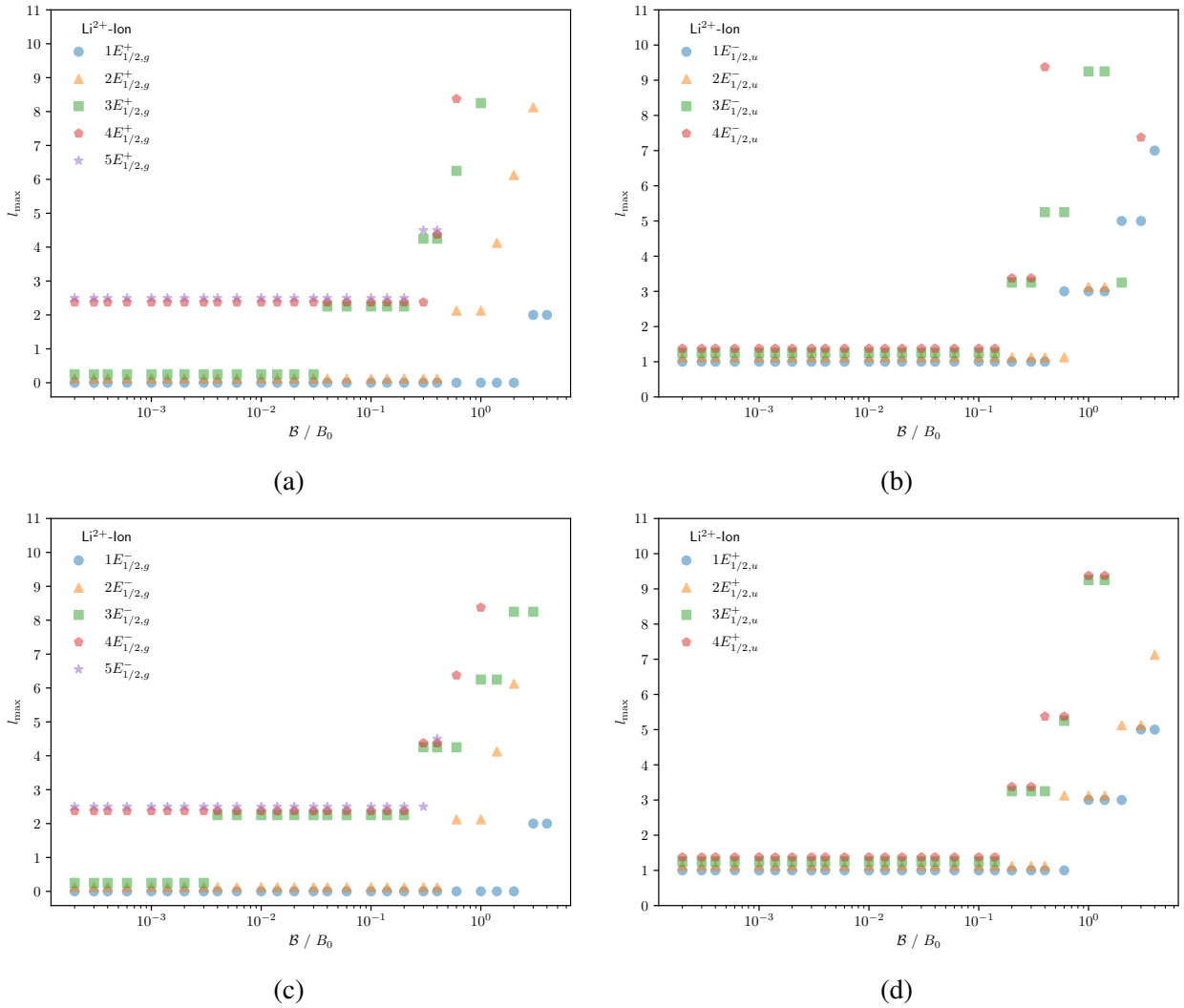

Figure 8: Basis set convergence for the $E_{1/2}$ states of Li^{2+}.

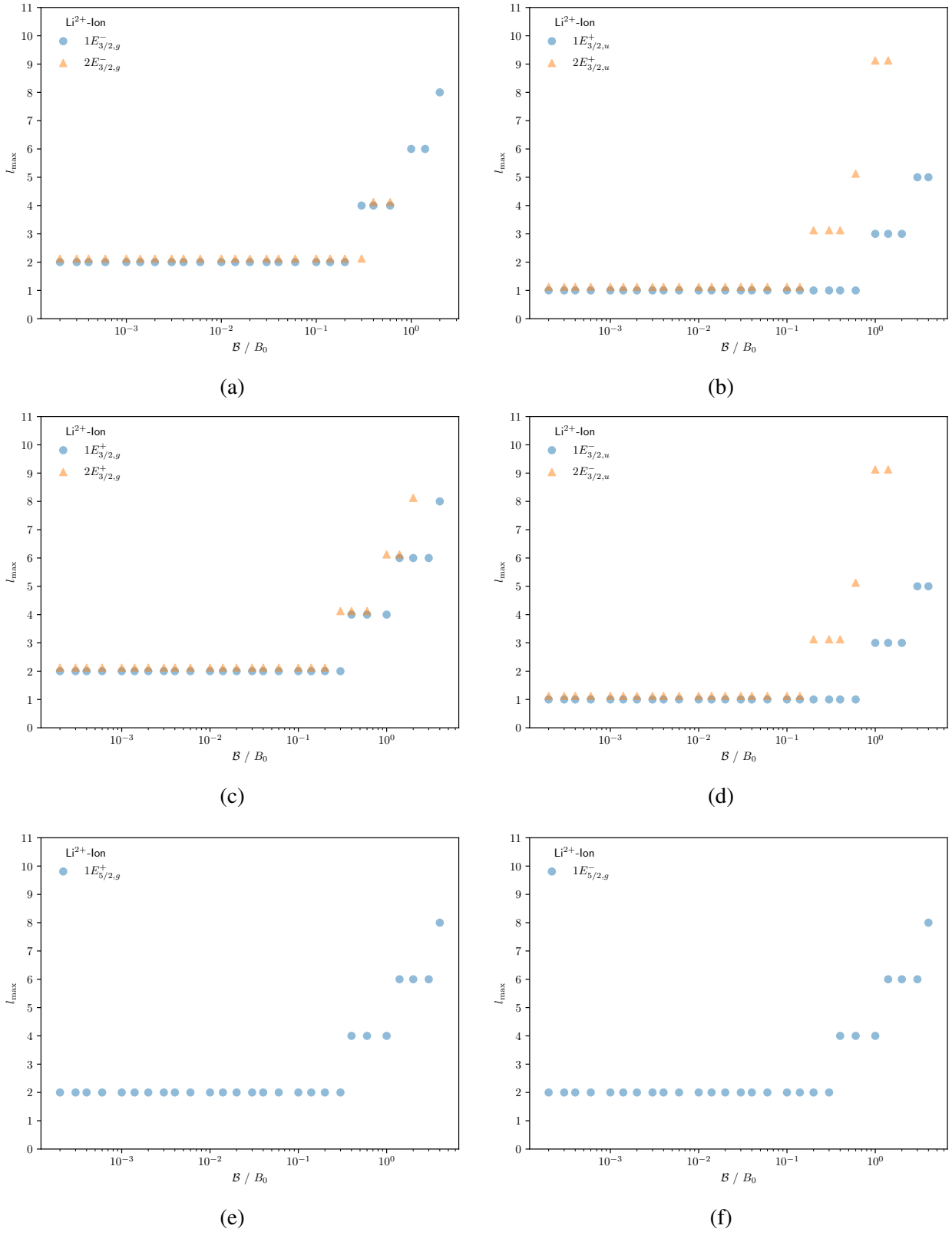

Figure 9: Basis set convergence for the $E_{3/2}$ and $E_{5/2}$ states of Li^{2+}.

7.3 The Na^{10+} ion

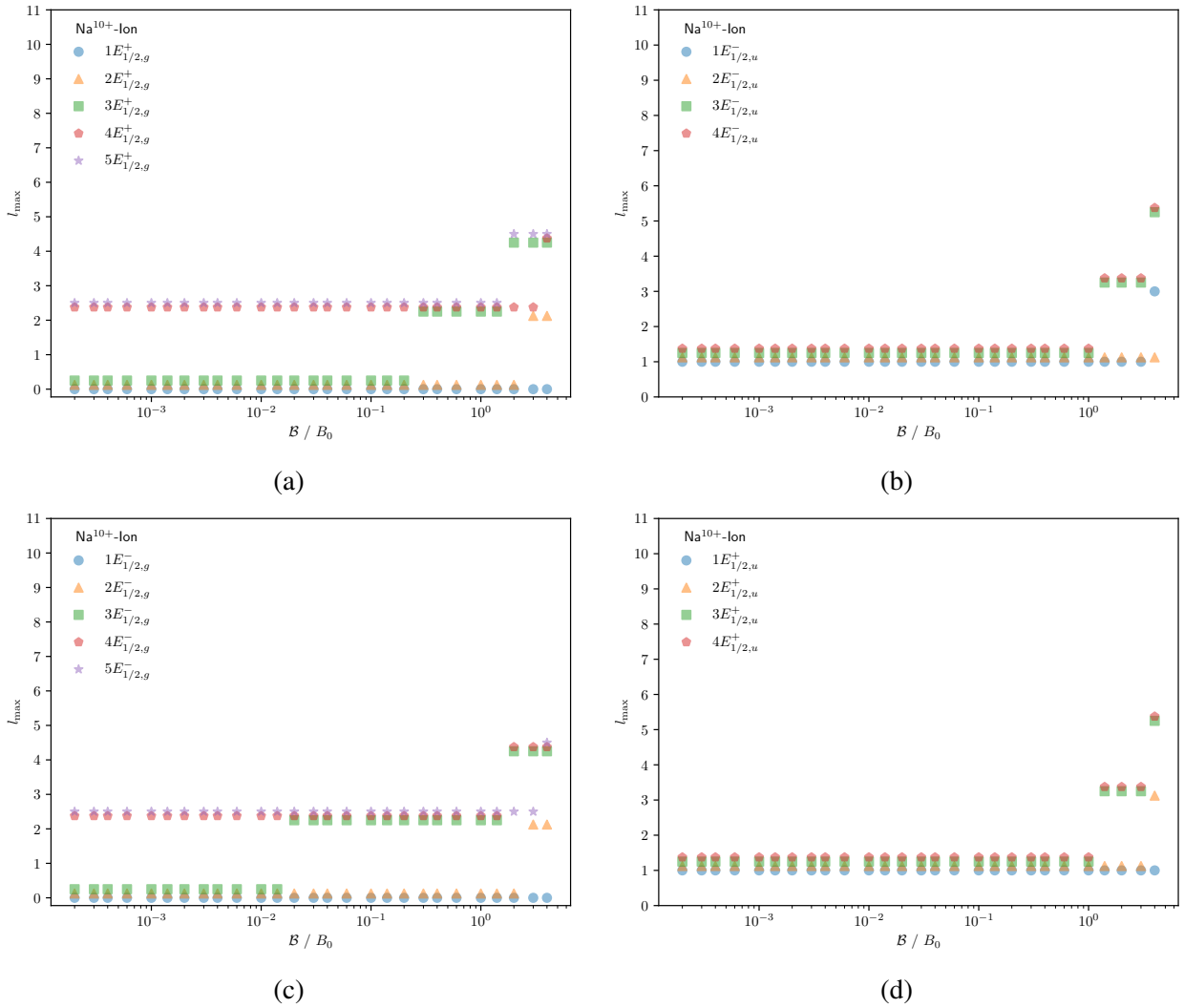

(a) (b)

(c) (d)

Figure 10: Basis set convergence for the $E_{1/2}$ states of Na^{10+}.

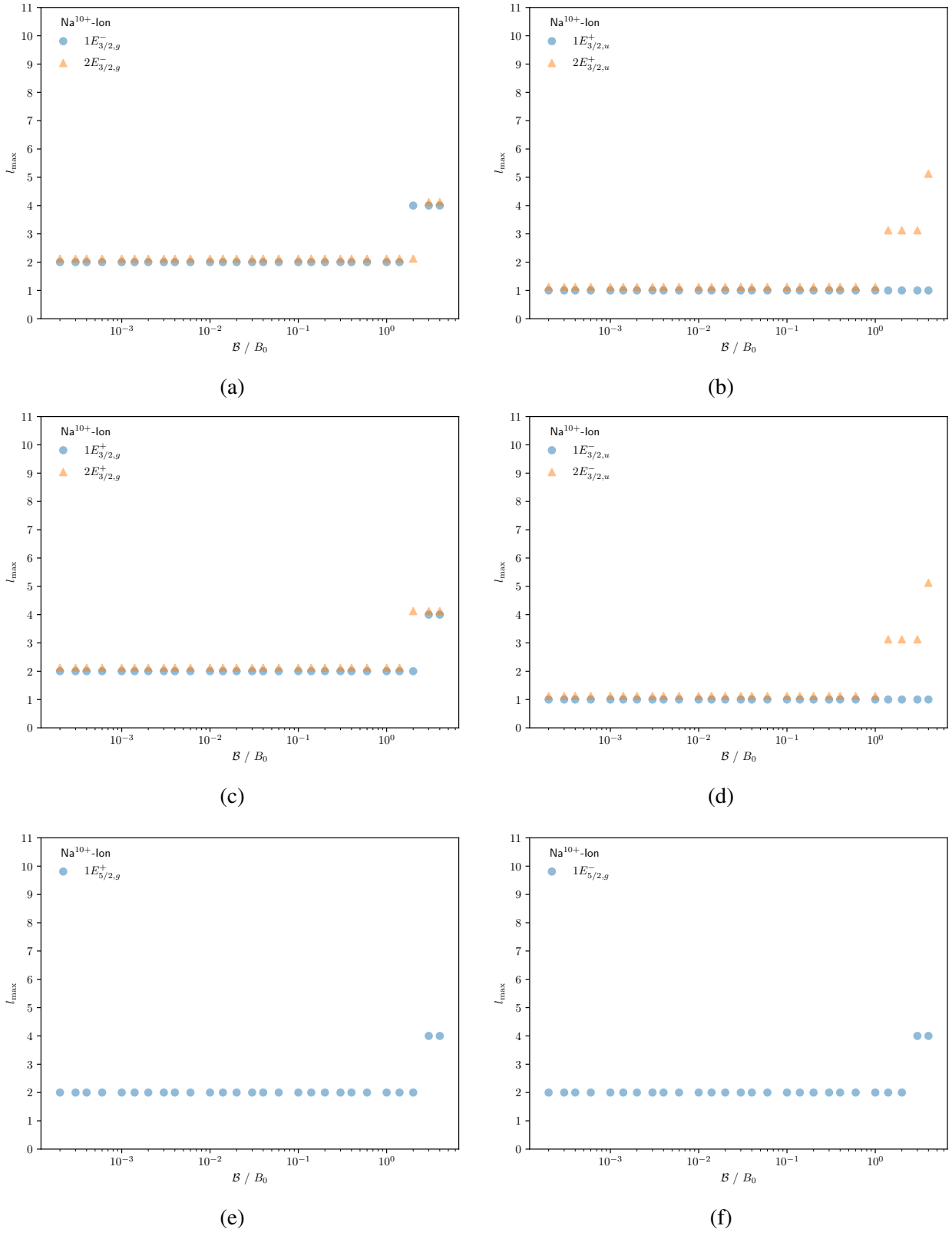

Figure 11: Basis set convergence for the $E_{3/2}$ and $E_{5/2}$ states of Na^{10+}.

7.4 The K^{18+} ion

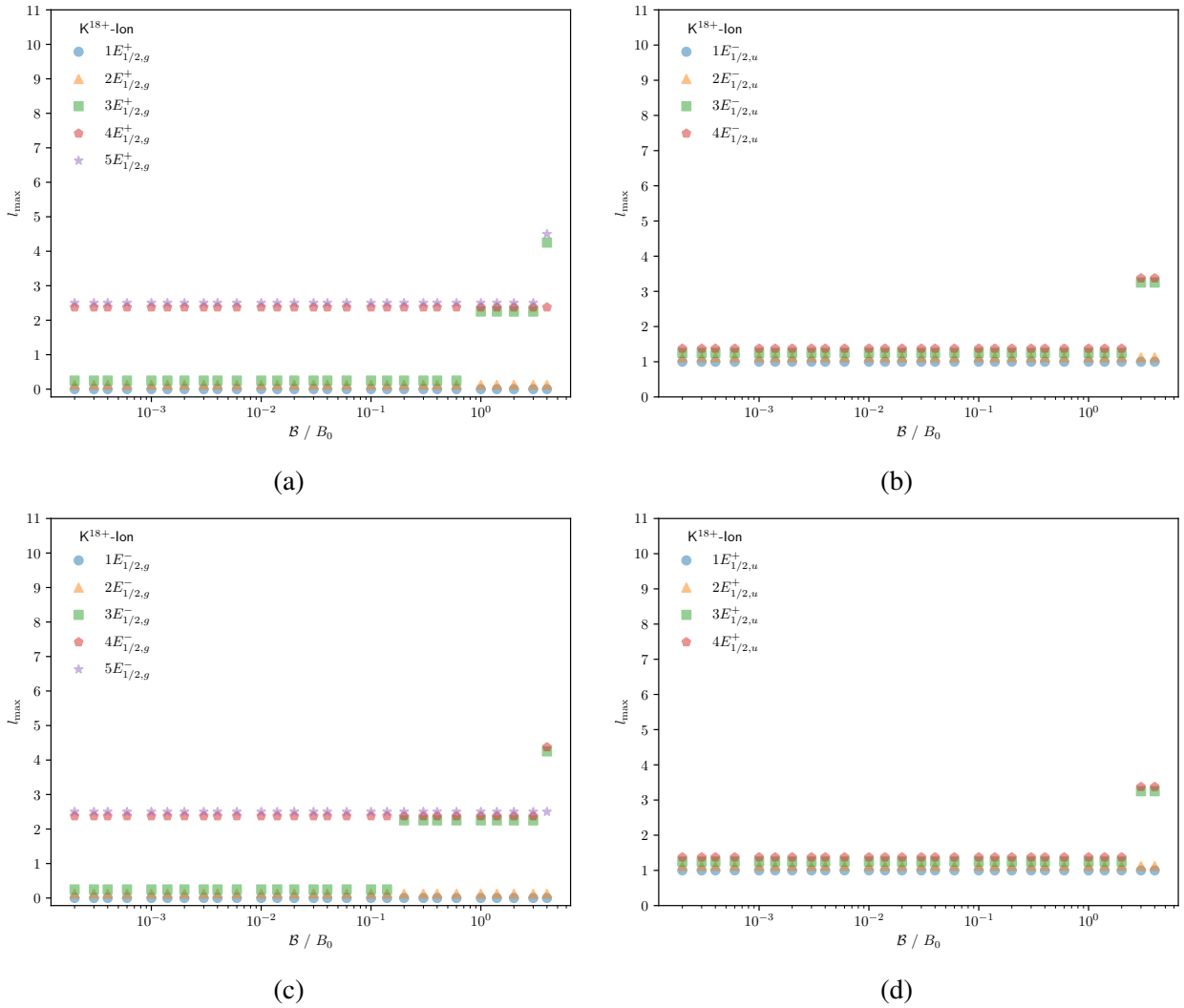

(a) (b)

(c) (d)

Figure 12: Basis set convergence for the $E_{1/2}$ states of K^{18+}.

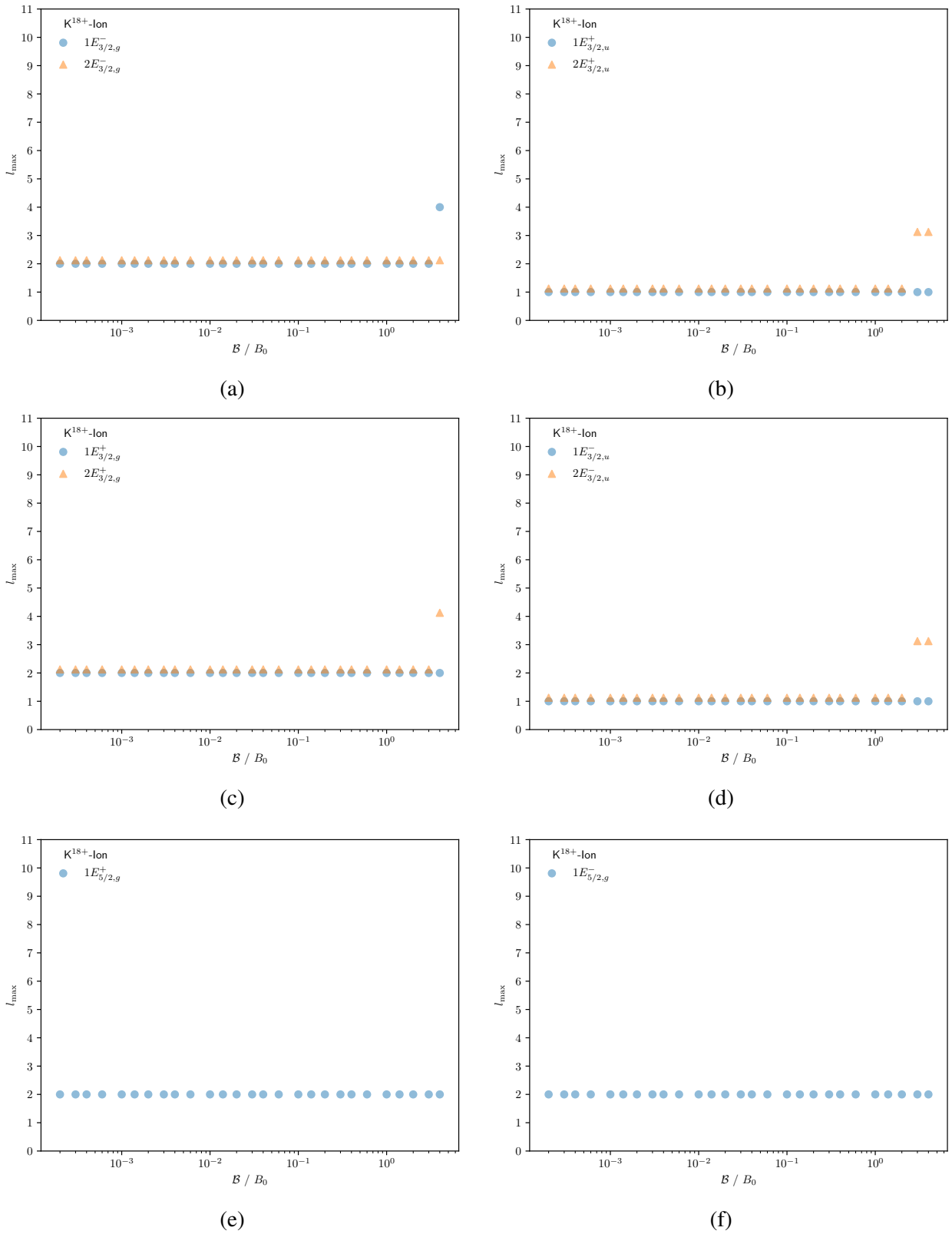

Figure 13: Basis set convergence for the $E_{3/2}$ and $E_{5/2}$ states of K^{18+}.

7.5 The Cu^{28+} ion

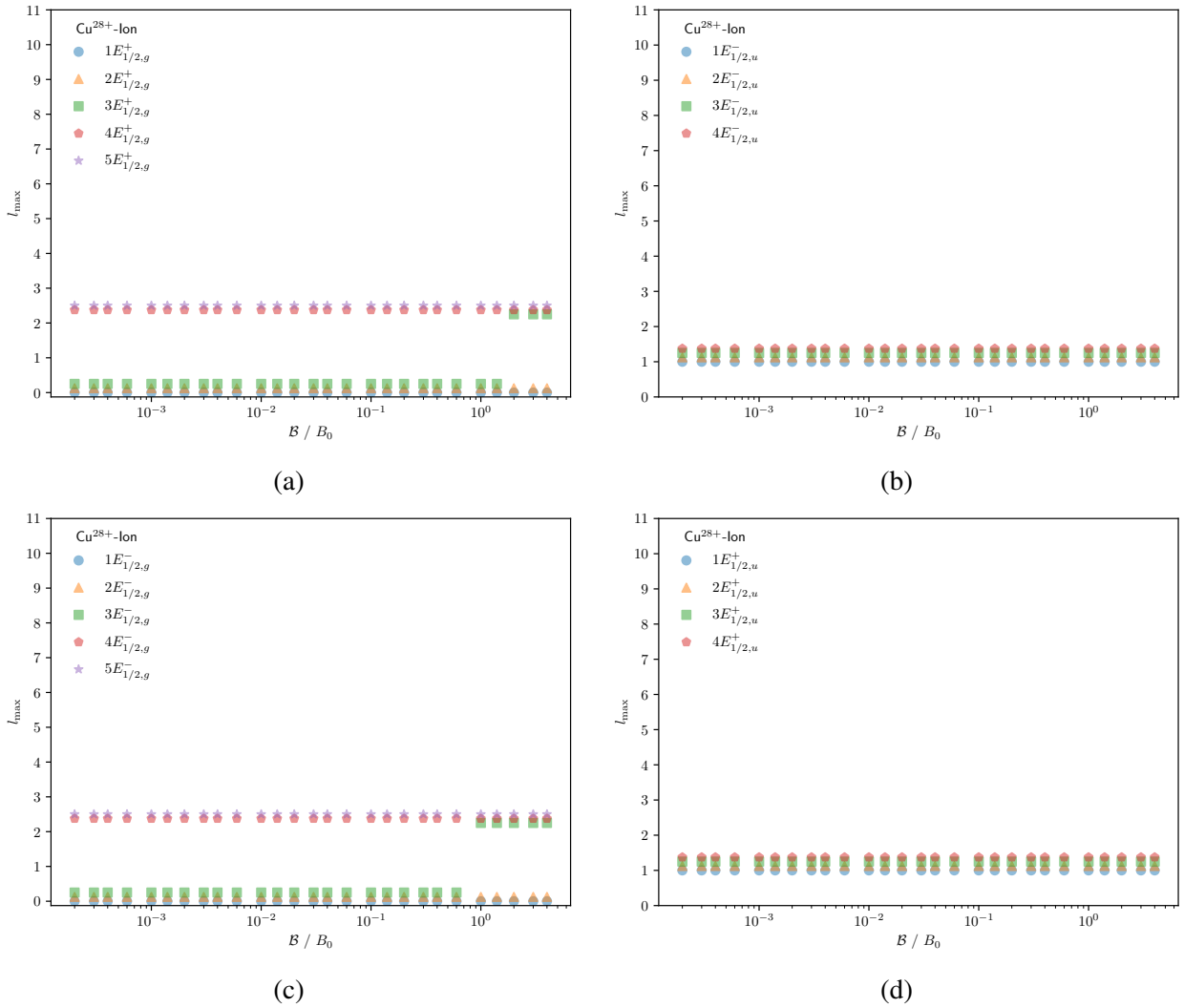

(a) (b)

(c) (d)

Figure 14: Basis set convergence for the $E_{1/2}$ states of Cu^{28+}.

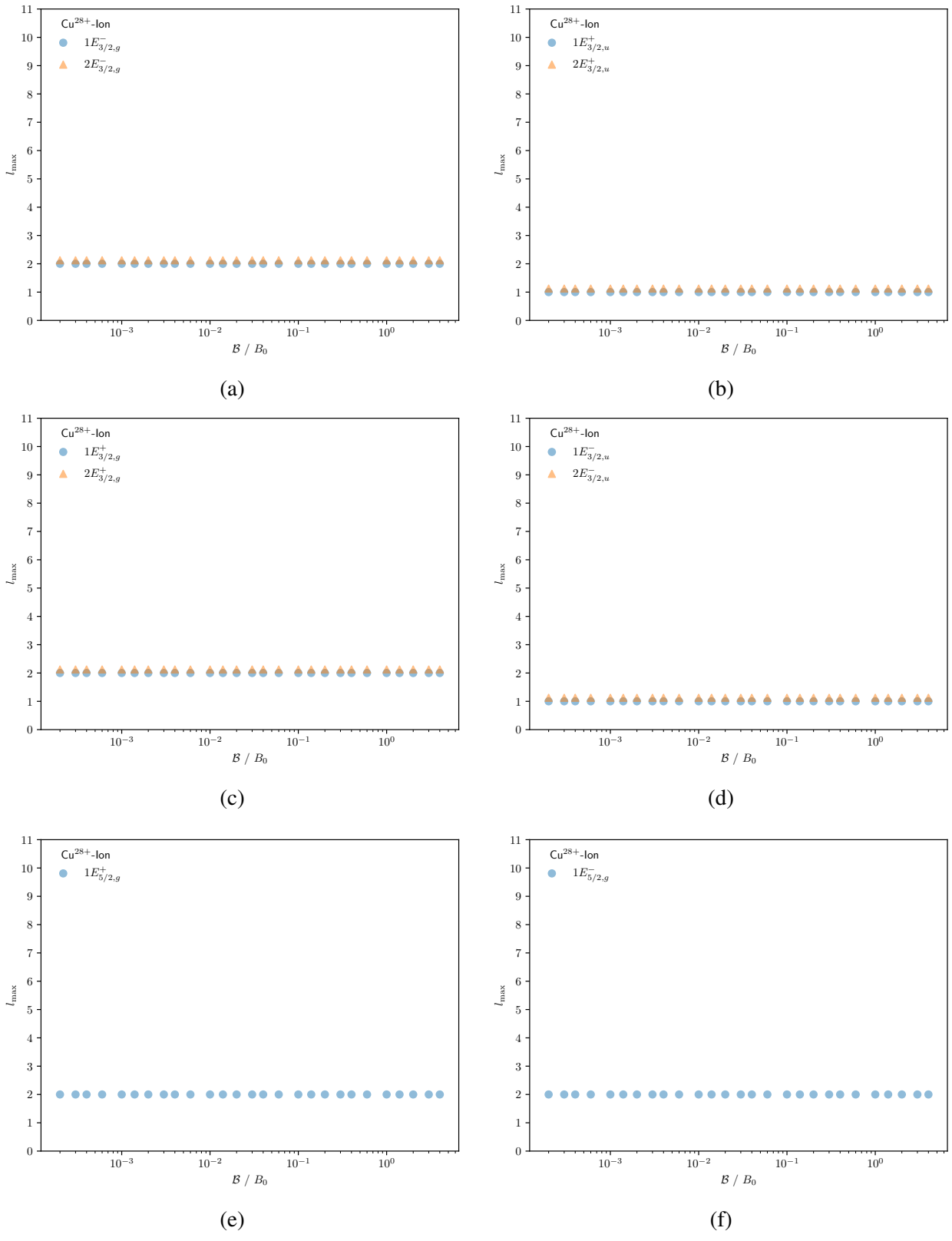

Figure 15: Basis set convergence for the $E_{3/2}$ and $E_{5/2}$ states of Cu^{28+}.

7.6 The Ag^{46+} ion

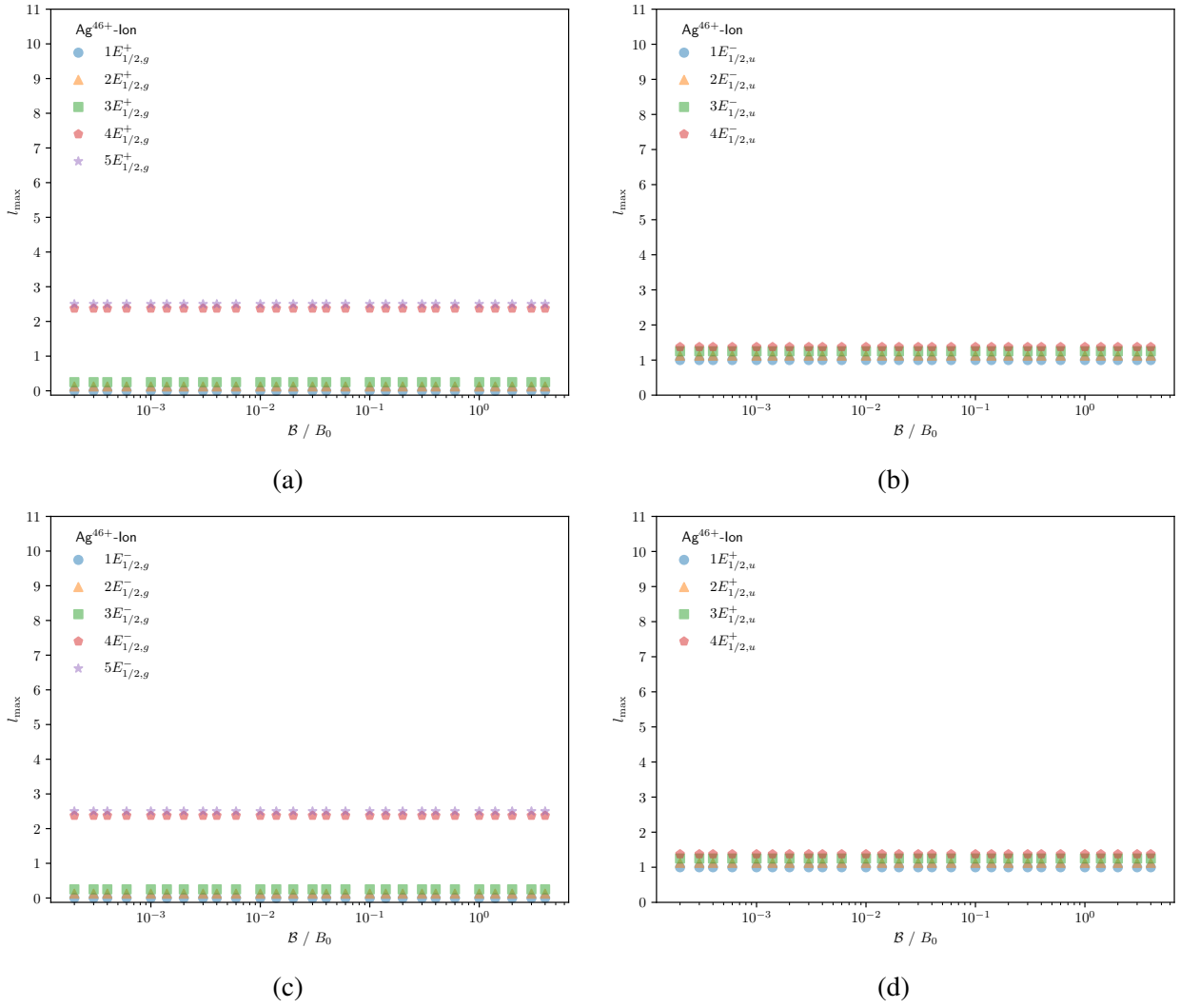

Figure 16: Basis set convergence for the $E_{1/2}$ states of Ag^{46+}.

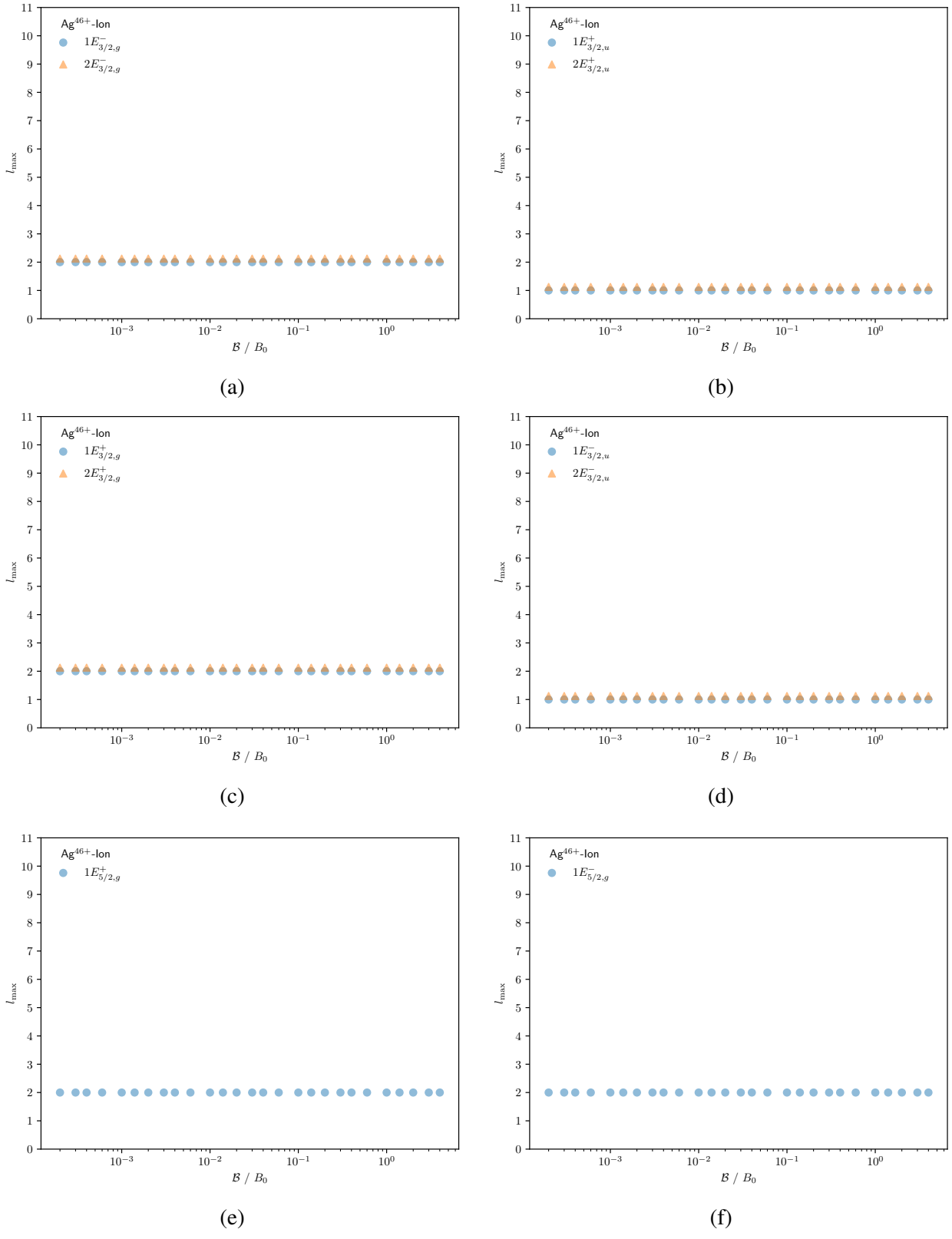

Figure 17: Basis set convergence for the $E_{3/2}$ and $E_{5/2}$ states of Ag^{46+}.

7.7 The Au^{78+} ion

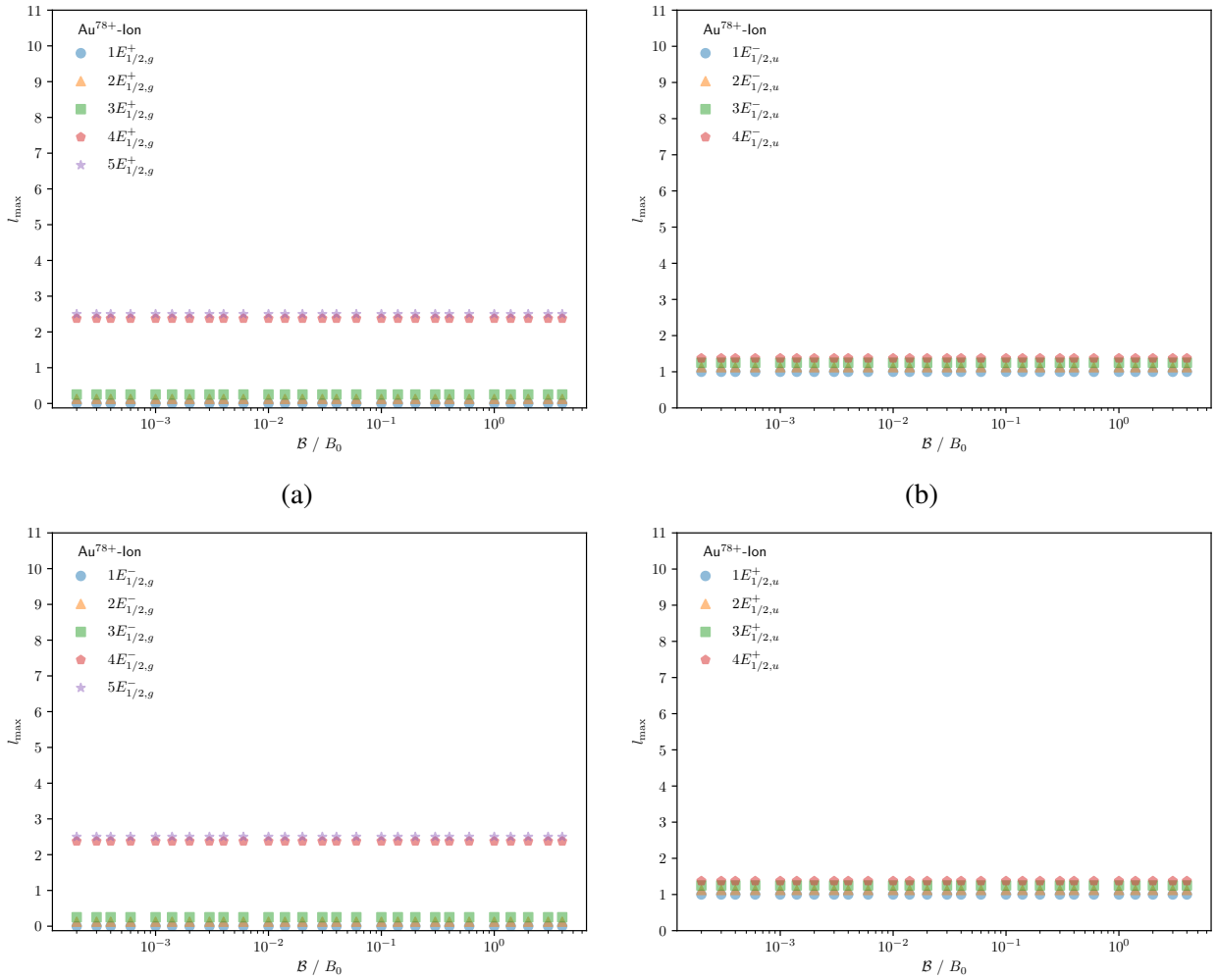

(a) (b)

(c) (d)

Figure 18: Basis set convergence for the $E_{1/2}$ states of Au^{78+}.

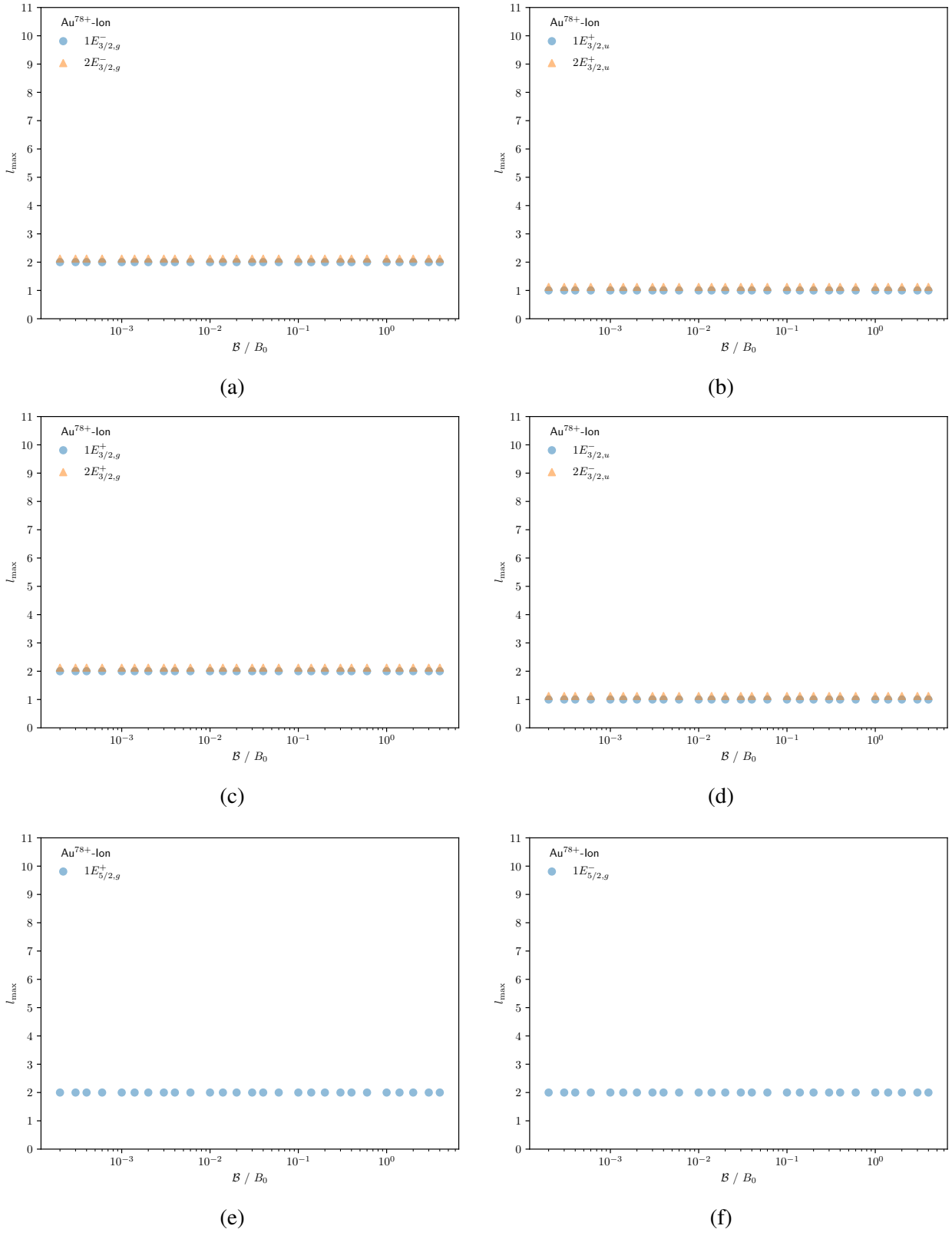

Figure 19: Basis set convergence for the $E_{3/2}$ and $E_{5/2}$ states of Au^{78+}.

7.8 The Rn^{85+} ion

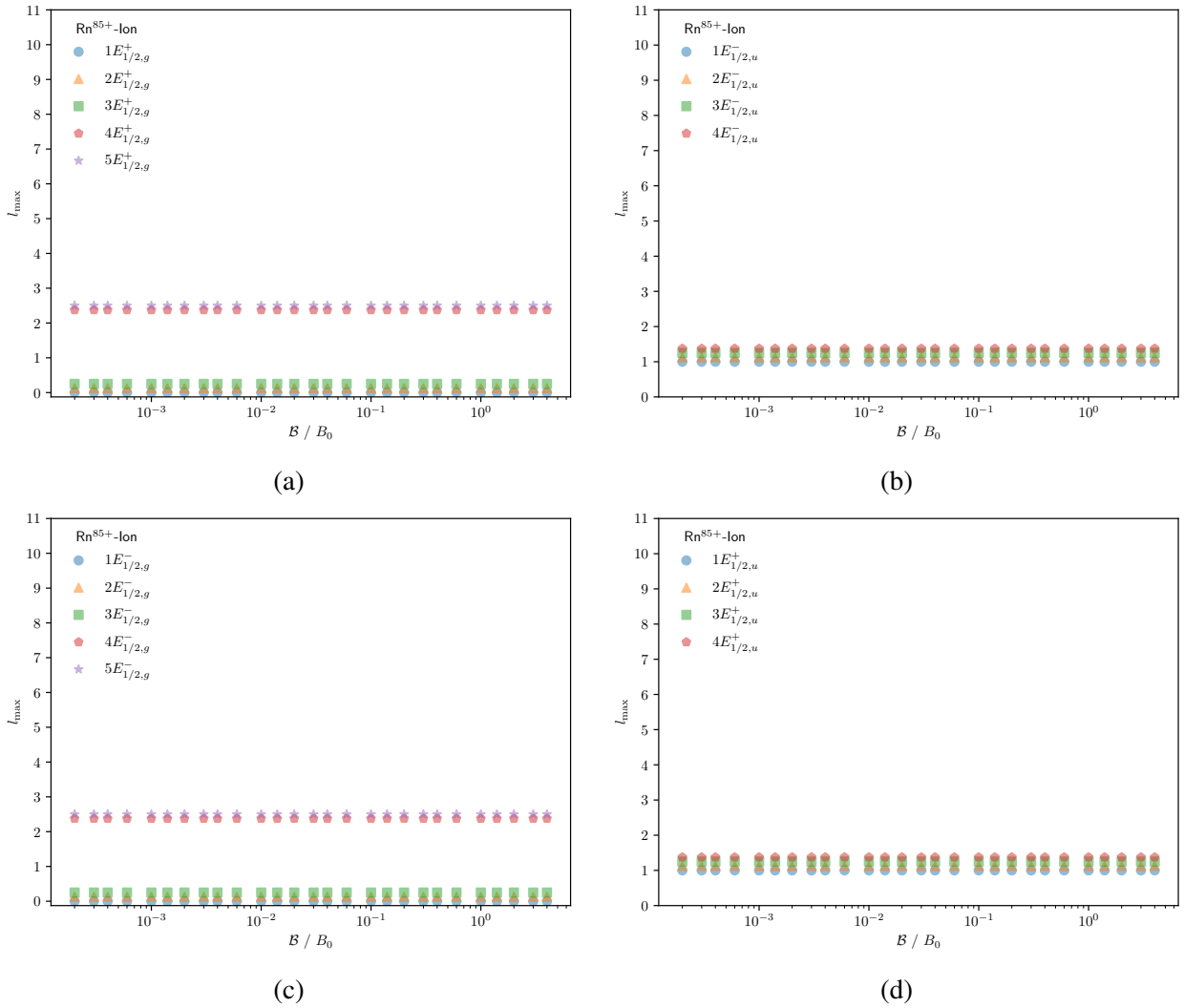

Figure 20: Basis set convergence for the $E_{1/2}$ states of Rn^{85+}.

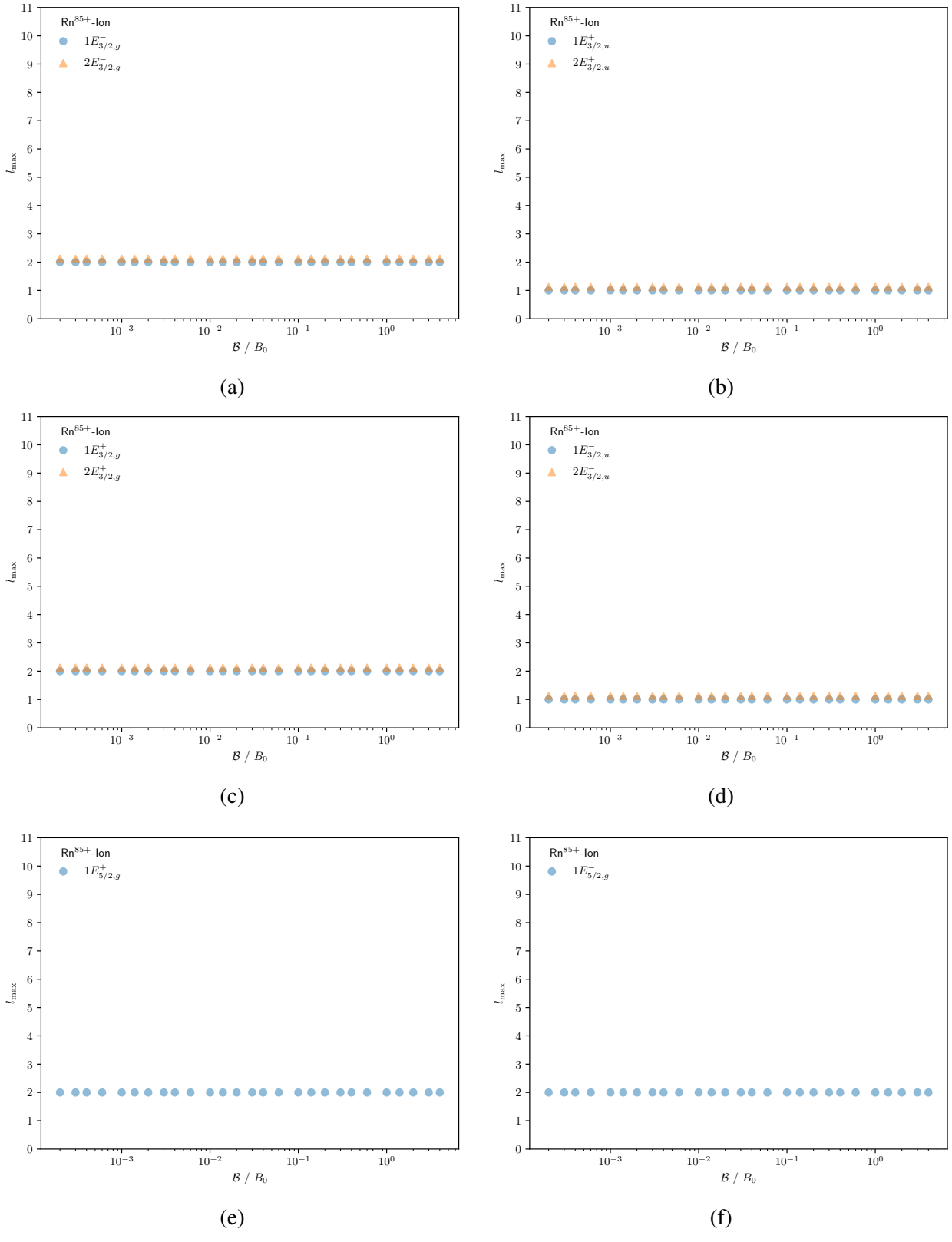

Figure 21: Basis set convergence for the $E_{3/2}$ and $E_{5/2}$ states of Rn^{85+}.

References

(1) Rösner, W.; Wunner, G.; Herold, H.; Ruder, H. Hydrogen atoms in arbitrary magnetic fields. I. Energy levels and wavefunctions. *J. Phys. B: Atom. Mol. Phys* **1984**, *17*, 29–52.

(2) Altmann, S. L. *Rotations, Quaternions, and Double Groups*; Dover Publications: Mineola, N.Y, 2005.